Research Square

Preprints are preliminary reports that have not undergone peer review.
They should not be considered conclusive, used to inform clinical practice,
or referenced by the media as validated information.

Reef resilience and demise on the NW shelf of Australia during the warm Miocene

Benjamin Petrick
benjamin.petrick@ifg.uni-kiel.de
Kiel University https://orcid.org/0000-0002-4211-0625
Lars Reuning
Kiel University
Or M. Bialik
Israel Oceanographic and Limnological Research
Lorenz Schwark
Kiel University
Miriam Pfeiffer
Kiel University

Research Article

Keywords:

Posted Date: August 28th, 2026

DOI: https://doi.org/10.21203/rs.3.rs-10804107/v1

License: This work is licensed under a Creative Commons Attribution 4.0 International License. Read Full License

Additional Declarations: The authors declare no competing interests.

Abstract

During the Miocene, sea surface temperature (SSTs) and CO_2 exceeded modern levels. Given the current decline of coral reefs due to rising summer temperatures, it is unclear how extensive reef systems developed and thrived in a warm Miocene world. This problem is exacerbated by a lack of SST reconstructions. Here, we use TEX_{86}^H to reconstruct summer SSTs between 5.0-17.4 Ma from a sediment core (IODP Site U1464) within the Miocene NW Australian shelf Barrier Reef system. During the Miocene Climate Optimum, summer SSTs reached up to 34 ºC. However, stable arid conditions and low subsidence rates allowed the reef to expand. Around 6 Ma, SSTs were ideal for coral reef growth, but increased terrestrial input and subsidence caused the relatively rapid collapse of almost all reefs. Multiple environmental stressors culminated in reef drowning. Therefore, a barrier reef system formed at > 30 °C SSTs, but this was only possible under otherwise ideal conditions.

Teaser

A Miocene barrier reef in NW Australia thrived in high SSTs in otherwise ideal conditions but collapsed due to multiple stressors during a cooler climate.

Introduction

Coral reefs are among the most diverse and ecologically significant marine ecosystems, yet they are known for their sensitivity to rising sea surface temperatures (SSTs) [1].

Coral forms structurally complex habitats that foster biodiversity and provide important ecosystem services essential to human society [2,3]. The monetary value of these ecosystem services is higher than that of any other biome on earth [4] and has been valued at approximately US$10 trillion per year worldwide [5]. It is therefore alarming that coral reefs are in decline. The global coverage of tropical coral reefs and their ability to provide ecosystem services have declined by half since the 1950s [6]. In fact, these ecosystems are globally the most affected by anthropogenic ocean warming [7].

Although recent extreme climatic events have triggered widespread coral bleaching [8,9], the thermal tolerance of corals and coral reefs in the geological past may have exceeded that of most modern reefs. Moreover, evidence from contemporary systems indicates that, while elevated SSTs are a major driver of bleaching, other stressors, such as suspended sediment concentrations, can locally be equally important [10].

The geological record offers a striking illustration of this complexity. Coral reefs persisted and even flourished through warm intervals of the Cenozoic [11,12]. Notably, Indo-Pacific reefs reached their maximum aerial extent during the Miocene Climatic Optimum (MCO) between 17-14 Ma (millions of years ago) [11], a period characterized by elevated global temperatures and atmospheric CO_2 concentrations comparable to projections for the end of this century [13–15]. Paradoxically, these same reef systems collapsed during the Late Miocene Cooling (LMC) [16], during which SSTs were either similar to or slightly colder than modern values [16–18].

This contrast presents a central conundrum: how did coral reefs thrive under the warmer-than-modern conditions of the MCO, yet fail during the comparatively moderate LMC? Resolving this paradox is essential for understanding both the resilience of coral reefs to future warming and their vulnerability to collapse under additional environmental stressors.

The Miocene “Great Barrier Reef” on the Northwest Shelf of Australia [19,20] provides an ideal case study to address this research gap (Fig. 1). Its extent and evolutionary history are well constrained by previous seismic studies [19–24]. IODP Site 1464 is the only site where a drill core has been recovered for scientific purposes that sampled sediments adjacent to the Miocene “Great Barrier Reef” across both the MCO and LMC, thus covering the period during which the reef developed. This offers a unique opportunity to link the Miocene core record to the seismic expression of reef initiation, growth, and demise [20]. Building on this foundation, we combine previous work on the reef’s development and drowning throughout the Miocene with a new biomarker-based SST record to evaluate how the reef responded to warmer conditions during the MCO and why it ultimately drowned during the LMC. The objectives of this study are (1) to quantify the temperatures experienced by the reef during the MCO and (2) to determine the factors that led to its final demise between 7–5 Ma during the LMC.

Geological setting

The Miocene Barrier Reef on the Northwest Shelf of Australia (NWBR) [19–24,27] was an extensive reef and carbonate platform system extending across most of the NW Australian shelf, as identified in seismic and well data (Figs. 1, 2). Estimates based on seismic data indicate that the NWBR was comparable in size to the modern Great Barrier Reef (GBR) [19], even though the exact lateral extent is debated [28,29]. [19,20] tied the seismic development of the reef system to Site U1464 (Fig. 2). Based on this correlation and additional tie to industry wells [21,22,24], the NWBR developed from ~18 Ma to ~6 Ma.

The NWBR was interpreted as coral dominated barrier reef systems due to seismic criteria and well data, as summarized in [19,20]: Miocene “colonial coral boundstone” was described from industrial wells Basset-1A, Caswell-1 and Scott Reef-1 in the Browse Basin [30] and abundant massive and branching coral debris from Early to Middle Miocene cuttings of industrial wells Pascal 1 and Lucas 1 in the Bonaparte Basin [31].

Corals were widespread, abundant and diverse throughout the region of SE Asia and northern Australia during the Neogene [32]. These Miocene reefs contained many genera and species that are still found today, as well as all major growth forms characteristic of the modern Indo-West Pacific coral fauna [33]. Coral dominated systems also tend to develop specific morphologies, such as higher-relief buildups, pinnacle reefs, barrier reefs, more extensive platforms

and atolls, while larger foraminifer and algal dominated systems develop low-relief carbonate platforms [32]. These morphologic criteria characterized the NWBR since its initiation in the Early Miocene and have been used to interpret it as coral dominated system from high resolution 3D seismic data[19,20,24].

Well-expressed reefal systems first developed at ~18 Ma [24], and then by ~16 Ma, an extensive NWBR system had been established [19–24]. Between 15-12 Ma, during the late MCO and the Middle Miocene Climate Transition (MMCT), the NWBR reached and maintained its maximum extent, at least at its northern end (Fig. 3). This indicates that the reef could keep up with relative sea-level changes during this time (Fig. 2) [24]. However, between ~11-10 Ma, the seismic data indicate backstepping, suggesting that the vertical growth potential of the reef was outpaced by relative sea-level rise [19,20,24]. This culminated in the partial drowning of the barrier reef and marks the end of the large and extensive NWBR system [23,24]. By ~ 6 Ma, during the LMC, the system had increasingly transitioned into isolated atolls, some of which still exist today [20,23,24].

Results

[2736] The glycerol dialkyl glycerol tetraethers (GDGT) based paleotemperature proxy TEX_{86} is typically used in open ocean settings. However, marine sedimentary GDGT distributions can be influenced by non-temperature related environmental factors [37]. Thin-sections and high-resolution core image scans were used to evaluate the relationship between sedimentary facies and GDGT distribution. This interpretation was supported by seismic data presented by [20], which further constrain the depositional environment (Fig. 2).

The lowermost part of the succession (U1464C-56R to 43R, 832.90 to 705.70 mbsf; ~17.4 -15.4 Ma) is characterized by bioclastic pack- to grainstone with large benthic foraminifera, coralline algae, echinoderm fragments, bryozoa, and scarce planktonic foraminifera (Suppl Fig. S4). A seismic correlation shows that this unit was deposited offshore to the first Miocene coral reef build-ups, shallowing upward from a fully marine, marginal slope to a subtidal platform environment (Fig. 2). The high TEX_{86}-derived temperatures between 34-31 °C in this interval therefore represent unrestricted, open ocean temperatures from the MCO. The following interval (U1464C-42R to 3R, 696.43 to 317.70 mbsf, ~15.4 to 6.0 Ma) shows alternating beds with variable textures from peloidal mudstone to bioclastic grainstone with abundant large benthic foraminifera (Suppl Fig. 3; Fig. 3). This unit also contains most of the tropical corals recovered directly at Site U1464. These corals likely grew in the shallow lagoon behind the reef. They are heavily altered and partially replaced by gypsum and dolomite, preventing detailed taxonomic analysis; however, the assemblage includes the common reef-building genera *Acropora* and *Porites*. [35]. The seismic-to-well tie (Fig. 2) indicates that this unit was mainly deposited in a shallow sub-tidal, lagoonal backreef environment during a time of prolific reef growth. Dark algal mats and lenticular gypsum/anhydrite represent the shallowest part of the record, an intertidal to supratidal sabkha environment (Suppl Fig. 3; Fig. 3).

Starting at ~ 6.0 Ma (U1464B-34H, 306.88 mbsf) the lack of corals and an increase in the abundance of planktonic foraminifera and nannofossils, indicates a change to more pelagic sedimentation (Fig. 3). This change to deep-subtidal conditions is paralleled by a relative increase in siliciclastic deposition as shown by the potassium and thorium component of the spectral gamma-ray log (Fig. 3). The seismic-to-well tie confirms that this interval is characterized by a drowning of the reef platform and a disintegration of the barrier reef system into smaller atolls.

Comparison of GDGT indices with sedimentary facies corroborates earlier observations from this site, indicating that sabkha-related bacterial/algal mats are characterized by elevated GDGT-0% index and Methane Index (MI) both of which are indicators of higher methanogenesis. There is also an increase in the Branched and Isoprenoid Tetraether (BIT) index, suggesting an increase in the amount of terrigenous material that could interfere with the TEX_{86}, and GDGT 2/3 index, which traditionally indicates a deeper water column production of GDGTs, although here it is more likely indicating a non-thermal amount of these compounds., This is accompanied by low #Rings tetra, which indicates the GDGTs were formed in the sediment, and Ring Index (RI) values indicating an abnormal molecular distribution [36] (For further explanation, see methods below). This distinctive GDGT signature—indicative of a non-thermal overprint from microbial/algal mats—occurs exclusively in the shallow subtidal–supratidal interval between 650 and 500 mbsf (Fig. 3) and would have introduced a spurious cold bias into the temperature reconstruction. Consequently, twelve samples were excluded from the temperature reconstruction based on this criterion and additional standard indicators of non-thermal GDGT alteration (see Methods). Recent work suggests that TEX_{86} in the paleo-record typically reflects summer temperatures. Periods of low nutrient availability may elevate TEX_{86} reconstructed SST, although the dimension of this effect currently remains undetermined [38,39]. The lack of a nutrient record for the Miocene from U1464 limits our ability to determine whether magnified warming is present.[39]While coral reefs live in a lower nutrient environment, they still need nutrients to survive, suggesting nutrient levels were not ultra-low during the Miocene [40–42]. Consequently, the warmest TEX_{86}-reconstructed SSTs might be influenced by a low-nutrient environment (see our interpretation of the sedimentary succession below and in the supplements, which include a detailed description of the sedimentary succession and biomarker indices). As a result, we interpret the data as reflecting summer temperatures, with up to 1-2 °C of exaggeration due to low nutrient conditions (i.e., within the published error for the proxy (Figs. 4,5)).

Overall, the average GDGT-reconstructed SST between 5.4-17.4 Ma was 30.5 °C with a standard deviation of 2.0 °C (n=66) (Figs. 3, 4). The record can be divided into three principal climatic periods: The MCO (17.5-14 Ma) with an average SST of 33.0 °C +/- 1.24 (n=23); The MMCT (14-12.5) with an average SST of 29.3 °C +/- 0.87 (n=4), and the post-MMCT from 12.5-5.4 Ma with an average SST of 29.3 °C +/- 1.17 (n=39).

Discussion

Tropical sea surface temperature and the evolution of the NWBR

Early Miocene-Miocene Climatic Optimum

The first extensive Miocene coral reefs developed on the northern NW Shelf of Australia at ~18 Ma, coinciding with the onset of the MCO [24]. High-quality seismic data indicate that the complete barrier system reached its maximum extent by 16-15 Ma [19–21,24].

Before ~17 Ma, summer SSTs were at the upper limit of the modern ideal reef growth window, meaning that annual SSTs were likely well within the window of ~ 25 to 29°C [44,45] (Fig. 4). The TEX_{86}^{H} summer SST reconstruction shows an increase from 31.0 °C at ~17.4 Ma to 34.1°C at 16.0 Ma. Between 15.9 Ma and 14.6 Ma, the TEX_{86}^{H} summer SSTs are on average higher and vary between 31.6 and 34.3°C. The temperature record (Fig. 4) does not cover the initial establishment of the Miocene reef system at ~18 Ma [24]. However, the observed temperature increase during the early part of the record (~17.4 to 16.0 Ma) may indicate that SSTs were just above the modern summer SSTs during the initial establishment of the reef system and therefore close to the ideal coral reef growth window (Fig. 4).

The highest TEX_{86}^{H} summer SSTs (> 33°C) during the MCO are restricted to the interval from 16.3 to 14.9 Ma (Fig. 4). Although slightly below the maximum bleaching threshold of some modern corals [50], these temperatures clearly exceed the optimal range for modern reefs (Fig. 4), even when considering the maximum 2.5°C combined instrumental and methodological uncertainty of TEX_{86}^{H} SST reconstructions [51]. This is confirmed by the high Mg/Ca-reconstructed temperatures from ODP site 761, which also suggest that average SSTs were just above the modern coral reef growth window (Fig. 5) [47,52]. SSTs during the MCO were also warmer than those in modern times (Fig. 4), indicating that the warming was not restricted to higher latitudes but also affected the tropics.

Some modern reefs with seasonal SSTs exceeding the optimal growth window exist, with the Red Sea and Persian Gulf providing the most important contemporary analogs. For example, in the Red Sea, coral reefs persist at annual average SSTs of up to 32°C and endure summer heat waves of 38°C for several weeks [53–55]. Corals from the Arabian/Persian Gulf area, which features the warmest ocean waters on Earth today, grow at sites where mean summer temperatures can be up to 35 °C [50]. It should be noted, however, that the reef-building coral genera found in these habitats (*Acropora* spp. and *Porites* spp.) are the same as those occurring in the less extreme environments of the Indo-Pacific Ocean. Genetic adaptations, together with shifts in algal symbionts and the bacterial microbiome, likely enabled these corals to thrive in such extreme environments [56–58]. Such adaptations cannot be observed in the fossil record, but we speculate that similar mechanisms helped the Miocene corals on the NW shelf to build extensive reef systems.

Aside from temperature, arid conditions as seen in the Red Sea today are considered ideal for corals because there are few other external stressors related to terrigenous sediment influx, and high salinity maintains high alkalinity [59–61]. However, these adaptations have some impacts, such as slower growth rates, which drop to almost zero when temperatures exceed average summer SSTs of 30°C [62,63]. Modern corals show reduced growth rates in response to elevated SSTs above the ideal coral growth window [45,64]. Evidence indicates that SSTs of 27-32°C led to a reduction in coral extension rates in the Caribbean and Northern Tethys Ocean during the Late Miocene [65,66]. In general, Miocene corals exhibit low growth rates [67] Therefore, summer SSTs between 31-34 °C may have resulted in lower coral extension rates at the NW Shelf of Australia in the Miocene. Other factors, such as coral cover, are equally important to coral extension rates for carbonate production in reefs [68–70]. However, a recent study from Oligocene and Miocene reef systems in the Mediterranean shows that coral extension rates can be a good predictor for gross reefal carbonate production [71], possibly because live coral cover is less variable than expected. Therefore, lower coral extension rates would not favor the development of large, complex reef structures such as barrier reefs. Yet seismic reconstructions of reef area indicate that extensive, architecturally complex reefs flourished on the NE shelf of Australia during the MCO (Fig. 2) [19,20,24]. Other carbonate producers in tropical carbonate systems often contribute significantly to reef carbonate production [72], but these typically have temperature limits similar to those of corals, e.g. [73]. Studies from neighboring Southeast Asia also show that the transition from larger foraminiferal- and algal-dominated systems to coral-dominated reefs at the Oligocene–Miocene boundary significantly increased the extent and accumulation rates of carbonates [32]. Corals, therefore, appear to have been the primary factor controlling carbonate accumulation rates in Miocene reefs across the region.

The growth of a modern tropical carbonate factory depends on a particular ecological space characterized by high available photosynthetic radiation and low turbidity [74]. The BIT index values are lower during coral reef initialization between 17.4 and 15.0 Ma (Figs. 2, 3), indicating low terrestrial input during the MCO. This is confirmed by low spectral gamma-ray-derived Th- and K values in this interval (Fig. 3) and data from Cape Range at the southernmost part of the NW shelf, which indicates an increase in aridification during the latest Early Miocene [75]. By the Middle Miocene, there is no siliciclastic input in the Cape Range region [28]. This matches findings from the IODP site U1464 core NGRL data (Fig. 3), as well as the presence of gypsum/anhydrite and high porewater salinities, which also indicate a dry Miocene period across Australia [34,76]. Regional aridity [29] led to low turbidity and high availability of photosynthetically available radiation, both essential for maintaining the tropical carbonate factory [77]. In consequence, a deep photic zone, combined with relatively low subsidence rates [23] during the MCO, allowed the reef to remain in the photic zone despite relatively low coral growth rates.

Finally, changes in aragonite saturation (Ω_{arg}) need to be considered. The MCO was marked by elevated atmospheric CO_2 levels, forcing lower surface water pH [78]. These lower pH values would, in turn, lower the $\Omega_{arg,}$ whereby the intensity of the suppression is temperature dependent (Fig. 6). At lower temperatures, such acidification would result in a significant reduction of Ω_{arg} to values that would not allow for corals to calcify [79,80]. However, at higher temperatures, the solubility of CO_2 would be lower, leading to degassing and increasing Ω_{arg}. This combination may allow for a “Goldilocks” range, in which the temperature pushes Ω_{arg} high enough to overcome the acidification induced by high atmospheric pCO_2. The relatively high temperatures, therefore, contributed to maintaining relatively high aragonite supersaturation despite decreased pH, helping the corals to calcify.

Yet despite evidence of an active reef system, the maximum extent of the NWBR occurs only after the initial cooling during the MMCT, the global cooling event at the end of the MCO [19,20]. At IODP site U1464, the occurrence of sabkhas appears to correspond to the maximum sea-level declines during the MMCT (Fig. 4). Boron isotope studies show a shift in the pH from 7.9 to 8.1 at ODP Site 761 between 14.5-13.5 Ma [78]. At IODP site U1464, the seismic data show

that the reef system expands and progrades laterally beyond the core site during this time, and the facies in the core transitions to a lagoonal one (Supplement) (Figs. 2, 3) [20,24] (Fig. 4). The TEX_{86}^{H}-derived SST record presented here indicates cooler temperatures closer to the modern ideal coral growth window. This may have stimulated faster coral growth during the cooling associated with the MMCT. However, as discussed in the supplement, it is unclear how much cooling the site experienced due to the presence of sabkha-derived GDGTs [36]. As shown in Figure 3, rapid changes in the depositional environment occurred, as indicated by both the microfacies analysis and the TEX_{86} index (See supplement for more detail). These facies changes may limit our ability to reconstruct SSTs via GDGT distributions during this time. However, reconstructed SSTs closely match those at offshore ODP Site 761 (Fig. 5), supporting that they are representative of SSTs on the NW Shelf of Australia [47,85].

During the Late Miocene, the seismic data are interpreted to show two reductions in reef extent (Fig. 2) [24]. The first is a backstepping event that occurred between 11-9 Ma, and the second is a drowning at ~ 6 Ma during the LMC (7-5.5 Ma) (Figs. 2,3,4) [19,20].

Previous studies have shown that subsidence rates in NW Australia increased at around 10 Ma [21,86]. This links to a backstepping event of the reef system on the NW-shelf between 11-9 Ma [19–24]. Previously, we proposed that elevated SSTs in the Coral Sea northeast of Australia reduced reef-accumulation rates. Combined with a tectonic event between 11-8 Ma, this ultimately triggered backstepping and eventual reef drowning [48]. A similar process likely affected the NW shelf, as temperatures before the backstepping event between 12-11 Ma are within a similar range to those at ODP site 811 (Fig. 5). However, as shown in the supplements, the part of the core where the backstepping occurs represents a very shallow lagoonal environment dominated by bioclastic sediments and microbial/algal mats that may have harbored organisms producing specific GDGTs independent of SST. Therefore, the paucity of SST data during the backstepping phase limits the robustness of this conclusion.

Finally, between 6-4 Ma, many of the coral reefs on the NW shelf of Australia drowned, leaving only isolated atoll reefs, some of which survive to this day (Fig. 3). Near Site U1464, the rapid ecosystem changes and barrier reef drowning occurred at ~6 Ma during the LMC (7.0-5.5), when the TEX_{86}^{H}-derived SSTs were comparable to or even cooler than modern summer SSTs on the NW shelf of Australia (Fig. 5). We note that during the LMC, a collapse in porcelaneous larger benthic foraminifera is also observed [72]. The LMC is associated with large-scale climatic changes across the Indo-Pacific [16]. In northwest Australia, it marks the onset of the Australian Humid Period (AHP) [87]. The exact timing of the AHP onset remains uncertain due to limited core recovery at several NW shelf sites, including IODP Site U1464 [27,87–89]. However, available evidence indicates that the AHP began before 6 Ma, possibly in response to changes in the position of the ITCZ around 7 Ma during the LMC [34,87,88]. At IODP site 1464 (Fig. 3), increases in terrigenous input are noted around 6 Ma in the spectral gamma-ray log values of Th+K [35]. The onset of the AHP was also accompanied by an increase in siliciclastic input at sites farther south of U1464, leading to the deposition of the Bare Formation [89]. At site U1461 (Fig. 5), the highest amount of riverine input occurs around 5 Ma [90]. A higher siliciclastic input increases turbidity and can be a significant stressor for coral reefs [10,91]. The onset of the AHP may have caused a rapid collapse of the reef system by reducing the depth of the photic zone. Therefore, the increase in terrestrial input likely contributed to the collapse of the coral reefs and the final drowning of the NWBR [16,24]. At the same time, the NW shelf depositional environment appears to have deepened, potentially linked to increased subsidence rates [92]. Therefore, the final drowning of the NWBR likely resulted from shoaling of the photic zone combined with increased subsidence, reducing the total available area reefs can inhabit, despite summer SSTs ideal for coral reef growth.

It is important to note that the “sudden” drowning observed at IODP site U1464 occurred over a time span of 100 kyr to 1 Myr. Thus, even if our study shows coral reefs thriving at high summer SSTs and drowning at temperatures closer to the ideal modern coral growth window, this does not serve as an analog for future climatic changes that occur over much shorter periods. However, despite this, the NBWR climate record emphasizes that temperature is not the only driver of coral reef drowning. Instead, several stressors may interact to cause coral reef loss [48,91]. Many of these stressors also impact modern coral reefs and may be exacerbated by global climate change [93]. Therefore, our record demonstrates the importance of minimizing additional stressors that negatively affect coral reef carbonate production in a warmer world.

Conclusion

Our study of the NW Australian shelf barrier reef demonstrates that a large, complex reef system can develop and thrive under summer temperatures exceeding the modern reef growth window, despite the well-known sensitivity of such ecosystems to elevated temperatures. This aligns with modern observations showing that corals can persist under very warm summer conditions when other environmental factors are favorable. The extensive barrier system on the NW Australian shelf likely developed during the warmer-than-present MCO period, when summer temperatures were at times above the optimal modern reef growth window. The arid conditions of the Middle Miocene may have alleviated additional stressors, such as turbidity and nutrient input. This allowed corals to persist and build extensive reef structures, even under sustained high temperatures that likely reduced coral growth rates. Yet, the largest barrier reef system formed during the MMCT, when summer SSTs were closer to the ideal modern reef growth window.

The onset of the Australian Humid Period triggered environmental changes - including increased river runoff and a shallowing of the photic zone – that led to the collapse of the barrier reef during the Late Miocene Cooling (~7 to 5 Ma). This illustrates that even extensive reef systems are vulnerable to environmental shifts, although the rates of the observed changes were much slower (> 100 kyr) than those experienced by modern reefs.

Overall, our results indicate that extensive Miocene coral reefs could thrive under higher than present summer SSTs in an otherwise optimal environment, absent other significant external stressors. The time scales during which the corals can adapt to these high summer temperatures are currently unclear. While our study seemingly gives hope for coral reefs in a warmer future world, current reef systems are exposed to much more rapid climatic changes. Importantly, anthropogenic warming is associated with multiple stressors, including rapid sea level rise, ocean acidification, increased pollution, and

terrigenous input due to coastal development. These interacting stressors can drive reef collapse, highlighting the importance of minimizing local and regional stressors to protect coral reef ecosystems in a warming world.

Methods

Sampling site

IODP Site U1464 was drilled at 264 m water depth during IODP Expedition 356 on the Northwestern Australian shelf [35]. Based on seismic data, the drill site was inferred to be situated on the landward side of a barrier reef system during the Miocene [19,20]. Facies analysis carried out onboard the JOIDES Resolution and post-cruise analysis verified that between 2.5 Ma and ~17 Ma, Site U1464 was in the vicinity of a reef system [20,34–36]. Evidence for this included the presence of zooxanthellate corals and other tropical shallow water biota (Gallagher et al., 2017a). Around ~14-12 Ma, sabkha deposits became more prevalent in the sediment recovered in the cores, indicating warm/arid peritidal conditions [34–36,76]. Previous work on the sabkha sediments showed that microbial mats related to sabkhas had a unique pattern of glyceroldialkylglycerolethers (GDGTs), which were not ideal for SST reconstruction [36]. Here, we focus on the entire period during which the NWBR was active (~5.4-17.4 Ma).

The age model for this locality is complicated by a lack of robust biostratigraphy, especially in the lower part of Hole U1464C. For Hole U1464B, we used the astronomically tuned age model of [27] For the samples from U1464C, the age model from [34] was used. Due to a lack of age model tie points, ages were extrapolated below 16 Ma. Therefore, the age of the sediments at the bottom of the core is uncertain but is estimated to be around 17.4 Ma, assuming constant sedimentation rates. However, no additional adjustments or tuning of the age model were performed. Depth in core is given as core depth below seafloor (CSF-A), reported as meters below seafloor (mbsf). A core composite depth below the seafloor (CCSF-A) is not available for Hole U1464C. Latitudinal reconstructions show that at 18 Ma the core site was located at a latitude of 24.4-26.6°S [94,95].

Organic geochemistry

For the TEX_{86}^{H} record, the TEX_{86} ratio being a well-established molecular paleothermometer [96], due to the low recovery of the Miocene section in Hole C (<25%), samples were selected from cores with sufficient material (5 cc) for biomarker analysis. The exception is the uppermost section (Hole B), where we tied the record to a previously published NGRL record [27] and used its peaks and troughs to guide sampling. We avoided Sabkha sediments as previous work showed they had an unusual GDGT signature and were not ideal for temperature reconstruction[36]. As shown below, the sabkhas still affected parts of the core we sampled. 73 samples were analyzed covering the time span from 5.4-17.4 Ma. We subsampled 20 cc of sediment, yielding approximately 20 g of sediment suitable for extracting sufficient total lipid extract for TEX_{86} determination. Dried and homogenized samples were Soxhlet extracted for 48 h using a solvent mixture of DCM and MeOH (9:1, v/v). The addition of activated copper turnings removed elemental sulfur. A Büchi solvent evaporator reduced the excess solvent to a final volume of 2 ml. Samples were then transferred into a 4 ml vial, where the total extract (TE) was taken to dryness under a gentle stream of nitrogen. TEs were fractionated into aliphatic, aromatic, and polar fractions by silica gel-column chromatography (6 ml SPE column, 2.8 g Silica 60 mesh, 25–40 µm) using solvents with increasing polarity in an LC-TECH automated SPE system. NSO containing (polar) compounds were eluted with 14 mL DCM/MeOH (1:1, v/v). The polar fraction was reconstituted in hexane/isopropanol (9:1, v/v) and re-chromatographed over aminopropyl-substituted silica gel (3 ml SPE column, 1.0 g aminopropyl-silica, 25–40 µm). The alcohol fraction containing the GDGTs used for TEX_{86}^{H} determination was eluted with 5 ml of hexane/isopropanol (9:1, v/v) and, after drying, was re-dissolved in hexane/isopropanol (99:1, v/v) to a final concentration of 6 mg/ml for injection into the HPLC/MS system.

GDGTs were measured on an AGILENT liquid chromatograph coupled to an AGILENT single quadrupole mass spectrometer following the analytical protocol of [97] The HPLC instrument was equipped with an AGILENT HILIC silica column (2.1 x 150 mm; 1.5 µm particle size) and a guard column maintained at 30°C. Detection of archaeal GDGT core lipids used for calculation of TEX_{86}^{H} was achieved by single ion recording of their protonated molecular ions [M + H^+], and compounds were quantified by integration of peak areas using AGILENT Masshunter© software. Because of the unique nature of the environment and to compare with previous records from the region, we used the TEX_{86}^{H}, which has proven robust in these environments [16,48,98–101]. All raw TEX_{86} data are provided in the supplement and can be recalculated if necessary. Calculation of TEX_{86}^{H} followed [43]. Reproducibility upon duplicate measurements showed a relative standard error of <2%.

The interval studied consists of sediments from various depositional environments around an active reef in a shallow-water setting, which differs from the open-ocean oceanic sediments where TEX_{86} was initially developed [96,102]. Furthermore, previous work on this core showed that the paleo-sabkhas were not appropriate for TEX_{86}-based SST reconstruction [36]. Therefore, extra care was taken to evaluate the effect of facies changes on the GDGTs and the TEX_{86}^{H} data.

To validate the GDGT-based SST reconstruction, we applied several GDGT indices that are commonly used to identify “non-thermally” produced GDGT distributions (Fig. S1). However, in doing this, we found that besides identifying SST data that may be affected by GDGTs found in sabkha sediments or parts of the core where there might be non-thermally producing GDGTs, these indices reflected changes in the facies in the core (See Supplement). The Methane Index (MI) was initially developed to indicate where GDGTs have been affected by gas-hydrate-related anaerobic oxidation of methane [103] (Fig. S1a). However, more recent work shows that it traces methane input in sedimentary environments [104]. The cut-off is debated, with polar sediments maybe being as low as 0.3 [37]. However, for non-polar sediments, the cut-off seems to be much higher at 0.5, which is what we have used here [104]. This led to 5 points being removed, all of which were associated with sabkha facies. The GDGT-0% index identifies samples with GDGTs that are substantially derived from sedimentary archaeal methanogenesis, especially methane clathrates (Fig. S1b) [105]. Given that previous work showed that sabkha sediments were defined

by high amounts of the molecule GDGT-0%, this is a particularly important test [36]. The cut-off for this index is >67%, and 7 sabkha samples failed this test. The branched and Isoprenoid Tetraether (BIT) index tracks the amount of terrigenous material that could interfere with the TEX_{86} values via soil-sourced GDGTs [96] (Fig. 3c). The cut-off for the BIT index is debated, and some researchers have suggested treating the data with caution. We have decided to use a cut of 0.45, which rejected 12 samples. We also combined the BIT with the $\#rings_{tetra}$ index, which was developed to understand how much of the branched GDGTs were being produced in situ versus those derived from terrigenous soil input [106] (Fig. S1e). It was recently proposed that when $\#rings_{tetra}$ is higher than 0.7, then the BIT index becomes invalid because most of the branched GDGTs were produced in situ [37,107]. This led to 3 samples being included despite high BIT. The Ring index (RI) was developed to evaluate whether the GDGTs deviate from normal open water oceanic values and thereby are created by the dominant GDGT producing *Nitrososphaera* archaea (formerly Thaumarchaeota) [108] (Fig. S1d). Samples are expected to fit within the 95% confidence interval, which is defined by ± 0.3 ΔRI units. This led to the rejection of 9 samples. Finally, the 2/3 index shows whether the GDGTs were being formed near the surface of the water column [109,110] (Fig. 3f). However, except for the samples taken directly from the sabkha associated microbial mats, all 2/3 values were below 3, indicating surface water production. In total, we removed 12 samples for SST analysis (Fig. S2), most of which failed multiple GDGT index quality analyses (high BIT, low $\#rings_{tetra}$, high %GDGT0, and high MI) (Figs. 3, S2), indicating influence of GDGTs distribution patterns by non-thermal processes . In the supplement, we discuss where the various samples were collected and how changes in facies affected the GDGT indices.

Declarations

Acknowledgements: We thank Sindia Sosdian for providing the Mg/Ca data for ODP Site 761. We would also like to thank the participants and staff on IODP Expedition 356 who helped collect the cores and provided background information on the cores in the initial reports. Also, thanks to the International Ocean Discovery Program for funding the expedition. Thanks to the Kochi core repository for providing the samples.

Funding Statement: This project was funded with a grant from the Deutsche Forschungsgemeinschaft (DFG) as part of the IODP grant program via project no. 447611930 awarded to Benjamin Petrick. Support for writing up was provided by a Humboldt Feodor-Lynen Fellowship awarded to Benjamin Petrick.

Author contributions: Both B.P. and L.R. contributed equally to the research and the writing of the paper. B.P. designed the project with the help of L.R. L.S. performed the biomarker analysis, and B.P. and L.S. interpreted the biomarker data. L.R. performed the facies and petrographic analysis. B.P. and LR worked on analyzing the facies data relationship to the biogeochemistry. O.B. did the carbonate geochemistry modeling. M.P. and L.R. helped with understanding reef dynamics. Lastly, B.P. and L.R. collaborated on the initial paper. B.P., O.B., and L.R. all drafted figures for the article. O.B., L.R., L.S., and M.P. provided valuable feedback on the article and assisted with editing.

Competing interests: The authors declare that they have no competing interests.

Data and materials availability: All data needed to evaluate the conclusions in the paper are present in the paper and/or the Supplementary Materials.

References

1. Roche, R. C., Williams, G. J. & Turner, J. R. Towards Developing a Mechanistic Understanding of Coral Reef Resilience to Thermal Stress Across Multiple Scales. *Current Climate Change Reports 2018 4:1* **4**, 51–64 (2018).
2. Hughes, T. P., Bellwood, D. R. & Connolly, S. R. Biodiversity hotspots, centres of endemicity, and the conservation of coral reefs. *Ecol. Lett.* **5**, 775–784 (2002).
3. Pendleton, L. *et al.* Coral Reefs and People in a High-CO2 World: Where Can Science Make a Difference to People? *PLoS One* **11**, e0164699 (2016).
4. de Groot, R. *et al.* Global estimates of the value of ecosystems and their services in monetary units. *Ecosyst. Serv.* **1**, 50–61 (2012).
5. Costanza, R. *et al.* Changes in the global value of ecosystem services. *Global Environmental Change* **26**, 152–158 (2014).
6. Eddy, T. D. *et al.* Global decline in capacity of coral reefs to provide ecosystem services. *One Earth* **4**, 1278–1285 (2021).
7. Hughes, T. P. *et al.* Coral reefs in the Anthropocene. *Nature 2017 546:7656* **546**, 82–90 (2017).
8. Duarte, G. A. S. *et al.* Heat Waves Are a Major Threat to Turbid Coral Reefs in Brazil. *Front. Mar. Sci.* **7**, 515393 (2020).
9. Gardner, S. G. *et al.* Coral microbiome diversity reflects mass coral bleaching susceptibility during the 2016 El Niño heat wave. *Ecol. Evol.* **9**, 938–956 (2019).
10. Fabricius, K. E. Effects of terrestrial runoff on the ecology of corals and coral reefs: review and synthesis. *Mar. Pollut. Bull.* **50**, 125–146 (2005).
11. Kiessling, W. & Flügel, E. Paleoreefs—a database on Phanerozoic reefs. in *Phanerozoic Reef Patterns* 77–92 (SEPM (Society for Sedimentary Geology), 2002). doi:10.2110/pec.02.72.0077.
12. Perrin, C. & Kiessling, W. Latitudinal Trends in Cenozoic Reef Patterns and their Relationship to Climate. in *Carbonate Systems during the Oligocene–Miocene Climatic Transition* 17–33 (Wiley, 2012). doi:10.1002/9781118398364.ch2.
13. Badger, M. P. S. *et al.* CO2 drawdown following the middle Miocene expansion of the Antarctic Ice Sheet. *Paleoceanography* **28**, 42–53 (2013).
14. Bolton, C. T. *et al.* Decrease in coccolithophore calcification and CO2 since the middle Miocene. *Nat. Commun.* **7**, 10284 (2016).
15. Steinthorsdottir, M. *et al.* The Miocene: The Future of the Past. *Paleoceanogr. Paleoclimatol.* **36**, (2021).
16. Petrick, B. F., Reuning, L., Pfeiffer, M., Auer, G. & Schwark, L. Impact of the Late Miocene Cooling on the loss of coral reefs in the Central Indo-Pacific. *Climate of the Past* **21**, 405–417 (2025).
17. Herbert, T. D. *et al.* Late Miocene global cooling and the rise of modern ecosystems. *Nat. Geosci.* **9**, 843–847 (2016).

18. Martinot, C. *et al.* Drivers of Late Miocene Tropical Sea Surface Cooling: A New Perspective From the Equatorial Indian Ocean. *Paleoceanogr. Paleoclimatol.* **37**, e2021PA004407 (2022).
19. McCaffrey, J. C., Wallace, M. W. & Gallagher, S. J. A Cenozoic Great Barrier Reef on Australia's North West shelf. *Glob. Planet. Change* **184**, 103048 (2020).
20. McCaffrey, J. C. *et al.* The Rowley Shoals atolls: Remnants of a Miocene great barrier reef on the north-west Australian margin. *Glob. Planet. Change* **245**, 104688 (2025).
21. Belde, J., Back, S., Bourget, J. & Reuning, L. Oligocene and Miocene Carbonate Platform Development In the Browse Basin, Australian Northwest Shelf. *Journal of Sedimentary Research* **87**, 795–816 (2017).
22. Rosleff-Soerensen, B., Reuning, L., Back, S. & Kukla, P. Seismic geomorphology and growth architecture of a Miocene barrier reef, Browse Basin, NW-Australia. *Mar. Pet. Geol.* **29**, 233–254 (2012).
23. Rosleff-Soerensen, B., Reuning, L., Back, S. & Kukla, P. A. The response of a basin-scale Miocene barrier reef system to long-term, strong subsidence on a passive continental margin, Barcoo Sub-basin, Australian North West Shelf. *Basin Research* **28**, 103–123 (2016).
24. Thronberens, S., Back, S., Bourget, J., Allan, T. & Reuning, L. 3-D seismic chronostratigraphy of reefs and drifts in the Browse Basin, NW Australia. *GSA Bulletin* **134**, 3155–3175 (2022).
25. Reagan, J. R. *et al.* World Ocean Atlas 2023. Preprint at (2023).
26. Schlitzer, R. Ocean Data View. *Ocean Data View* (2021).
27. Groeneveld, J., Vleeschouwer, D. De, McCaffrey, J. C. & Gallagher, S. J. Dating the Northwest Shelf of Australia Since the Pliocene. *Geochemistry, Geophysics, Geosystems* **22**, e2020GC009418 (2021).
28. Riera, R., Bourget, J., Håkansson, E., Paumard, V. & Wilson, M. E. J. Middle Miocene tropical oligotrophic lagoon deposit sheds light on the origin of the Western Australian coral reef province. *Palaeogeogr. Palaeoclimatol. Palaeoecol.* **576**, 110501 (2021).
29. Riera, R., Paumard, V., Bourget, J., Allan, T. & Lebrec, U. Evolution of the Exmouth-Barrow carbonate margin through the Miocene: Insights from 3D seismic data and field investigations (North West Shelf, Australia). *Sediment. Geol.* **449**, 106371 (2023).
30. Apthorpe, M. C. Cainozoic depositional history of the North West Shelf. *Proceedings of the Petroleum Exploration Society of Australia Symposium, Perth 1988* 55–84 Preprint at (1988).
31. Gorter, J. D., Rexilius, J. P., Powell, S. L. & Bayford, S. W. Late Early to Mid Miocene Patch Reefs, Ashmore Platform, Timor Sea - Evidence from 2D and 3D Seismic Surveys and Petroleum Exploration Wells. (2002).
32. Wilson, M. E. J. Global and regional influences on equatorial shallow-marine carbonates during the Cenozoic. *Palaeogeogr. Palaeoclimatol. Palaeoecol.* **265**, 262–274 (2008).
33. Wilson, M., Rosen, B., … R. H.-… and geological evolution & 1998, undefined. Implications of paucity of corals in the Paleogene of SE Asia: plate tectonics or centre of origin. *researchgate.netMEJ Wilson, BR Rosen, R Hall, JD HollowayBiogeography and geological evolution of SE Asia, 1998•researchgate.net* https://www.researchgate.net/profile/Brianroy-Rosen-2/publication/267260031_Implications_of_paucity_of_corals_in_the_Paleogene_of_SE_Asia_plate_tectonics_or_Centre_of_Origin/links/6463b36002c509of-paucity-of-corals-in-the-Paleogene-of-SE-Asia-plate-tectonics-or-Centre-of-Origin.pdf (1998).
34. Groeneveld, J. *et al.* Australian shelf sediments reveal shifts in Miocene Southern Hemisphere westerlies. *Sci. Adv.* **3**, e1602567 (2017).
35. Gallagher, S. J. *et al.* Site U1464. in (2017). doi:10.14379/iodp.proc.356.109.2017.
36. Petrick, B., Reuning, L. & Martínez-García, A. Distribution of Glycerol Dialkyl Glycerol Tetraethers (GDGTs) in Microbial Mats From Holocene and Miocene Sabkha Sediments. *Front. Earth Sci. (Lausanne).* **7**, 310 (2019).
37. Bijl, P. K. *et al.* Reviews and syntheses: Best practices for the application of marine GDGTs as proxy for paleotemperatures: sampling, processing, analyses, interpretation, and archiving protocols. *Biogeosciences* **22**, 6465–6508 (2025).
38. Tran, T. T., Tierney, J. E., Holbourn, A. & Rattanasriampaipong, R. Biomarker Constraints on Indo-Pacific Warm Pool Temperature During the Late Pleistocene: The Role of Orbital Forcing. *Paleoceanogr. Paleoclimatol.* **41**, e2025PA005276 (2026).
39. Rattanasriampaipong, R., Tierney, J. E., Abell, J. T. & Gilmore, L. D. A Nutrient Effect on the TEX86 Paleotemperature Proxy. *Geophys. Res. Lett.* **52**, e2025GL115237 (2025).
40. Morris, L. A., Voolstra, C. R., Quigley, K. M., Bourne, D. G. & Bay, L. K. Nutrient Availability and Metabolism Affect the Stability of Coral–Symbiodiniaceae Symbioses. *Trends Microbiol.* **27**, 678–689 (2019).
41. Wiedenmann, J. *et al.* Nutrient enrichment can increase the susceptibility of reef corals to bleaching. *Nature Climate Change 2012 3:2* **3**, 160–164 (2012).
42. Hallock, P. & Schlager, W. Nutrient Excess and the Demise of Coral Reefs and Carbonate Platforms. *Palaios* **1**, 389 (1986).
43. Kim, J.-H. *et al.* New indices and calibrations derived from the distribution of crenarchaeal isoprenoid tetraetherlipids: Implications for past sea surface temperature reconstructions. *Geochemica et Cosmochimica Acta* **74**, 4639–4654 (2010).
44. Laugié, M., Michel, J., Pohl, A., Poli, E. & Borgomano, J. Global distribution of modern shallow-water marine carbonate factories: a spatial model based on environmental parameters. *Sci. Rep.* **9**, 16432 (2019).
45. Sawall, Y. *et al.* Extensive phenotypic plasticity of a Red Sea coral over a strong latitudinal temperature gradient suggests limited acclimatization potential to warming. *Scientific Reports 2015 5:1* **5**, 1–9 (2015).
46. Miller, K. G. *et al.* Cenozoic sea-level and cryospheric evolution from deep-sea geochemical and continental margin records. *Sci. Adv.* **6**, (2020).

47. Sosdian, S. M. & Lear, C. H. Initiation of the Western Pacific Warm Pool at the Middle Miocene Climate Transition? *Paleoceanogr. Paleoclimatol.* **35**, e2020PA003920 (2020).
48. Petrick, B. *et al.* Warm, not cold temperatures contributed to a Late Miocene reef decline in the Coral Sea. *Sci. Rep.* **13**, 4015 (2023).
49. He, Y., Wang, H. & Liu, Z. Development of the Leeuwin Current on the northwest shelf of Australia through the Pliocene-Pleistocene period. *Earth Planet. Sci. Lett.* **559**, 116767 (2021).
50. Shuail, D. *et al.* Local bleaching thresholds established by remote sensing techniques vary among reefs with deviating bleaching patterns during the 2012 event in the Arabian/Persian Gulf. *Mar. Pollut. Bull.* **105**, 654–659 (2016).
51. Kim, J.-H. *et al.* New indices and calibrations derived from the distribution of crenarchaeal isoprenoid tetraether lipids: Implications for past sea surface temperature reconstructions. *Geochim. Cosmochim. Acta* **74**, 4639–4654 (2010).
52. Sosdian, S. M., Babila, T. L., Greenop, R., Foster, G. L. & Lear, C. H. Ocean Carbon Storage across the middle Miocene: a new interpretation for the Monterey Event. *Nature Communications 2020 11:1* **11**, 1–11 (2020).
53. Evensen, N. R. *et al.* Empirically derived thermal thresholds of four coral species along the Red Sea using a portable and standardized experimental approach. *Coral Reefs* **41**, 239–252 (2022).
54. Moustafa, Y. A., Pätzold, J., Loya, Y. & Wefer, G. Mid-Holocene stable isotope record of corals from the northern Red Sea. *International Journal of Earth Sciences 2000 88:4* **88**, 742–751 (2000).
55. Riegl, B. & Piller, W. E. Reefs and coral carpets in the northern Red Sea as models for organism-environment feedback in coral communities and its reflection in growth fabrics. *Geological Society, London, Special Publications* **178**, 71–88 (2000).
56. Hsieh, Y. E. *et al.* Successive responses of three coral holobiont components (coral hosts, symbiotic algae, and bacteria) to daily temperature fluctuations. *Ecol. Indic.* **158**, 111515 (2024).
57. Fiesinger, A. *et al.* Symbiodiniaceae shifts over the last decade on the hottest coral reefs on Earth. *Coral Reefs 2025 44:6* **44**, 2049–2064 (2025).
58. Howells, E. J. *et al.* Enhancing the heat tolerance of reef-building corals to future warming. *Sci. Adv.* **7**, (2021).
59. Fine, M. *et al.* Coral reefs of the Red Sea — Challenges and potential solutions. *Reg. Stud. Mar. Sci.* **25**, 100498 (2019).
60. Gegner, H. M. *et al.* High salinity conveys thermotolerance in the coral model Aiptasia. *Biol. Open* **6**, 1943–1948 (2017).
61. Osman, E. O. *et al.* Thermal refugia against coral bleaching throughout the northern Red Sea. *Glob. Chang. Biol.* **24**, e474–e484 (2018).
62. Cantin, N. E., Cohen, A. L., Karnauskas, K. B., Tarrant, A. M. & McCorkle, D. C. Ocean Warming Slows Coral Growth in the Central Red Sea. *Science (1979).* **329**, 322–325 (2010).
63. Ortiz, J. C., González-Rivero, M. & Mumby, P. J. Can a thermally tolerant symbiont improve the future of Caribbean coral reefs? *Glob. Chang. Biol.* **19**, 273–281 (2013).
64. Lough, J. M. & Cantin, N. E. Perspectives on massive coral growth rates in a changing ocean. *Biological Bulletin* **226**, 187–202 (2014).
65. Brachert, T. C. & Schwark, L. Elevated Tropical Sea Surface Temperatures During the Globally Warm Miocene Caused Heat Stress for Caribbean Coral Reefs. *Terra Nova* **37**, 35–40 (2024).
66. Reuter, M. *et al.* Mid-Miocene warmth pushed fossil coral calcification to physiological limits in high-latitude reefs. *Communications Earth & Environment 2025 6:1* **6**, 569- (2025).
67. Brachert, T. C. *et al.* An assessment of reef coral calcification over the late Cenozoic. *Earth. Sci. Rev.* **204**, 103154 (2020).
68. Perry, C. T. *et al.* Loss of coral reef growth capacity to track future increases in sea level. *Nature 2018 558:7710* **558**, 396–400 (2018).
69. Perry, C. T. *et al.* Remote coral reefs can sustain high growth potential and may match future sea-level trends. *Scientific Reports 2015 5:1* **5**, 18289- (2015).
70. Perry, C. T. *et al.* Estimating rates of biologically driven coral reef framework production and erosion: a new census-based carbonate budget methodology and applications to the reefs of Bonaire. *Coral Reefs 2012 31:3* **31**, 853–868 (2012).
71. Kiessling, W. *et al.* Census-based estimates of Mediterranean Oligocene–Miocene reef carbonate production. *Facies 2024 71:1* **71**, 2- (2024).
72. Bassi, D. *et al.* Porcelaneous larger foraminiferal responses to Oligocene–Miocene global changes. *Palaeogeogr. Palaeoclimatol. Palaeoecol.* **634**, 111916 (2024).
73. Kinoshita, S. *et al.* Temperature effects on the shell growth of a larger benthic foraminifer (Sorites orbiculus): Results from culture experiments and micro X-ray computed tomography. *Mar. Micropaleontol.* **163**, 101960 (2021).
74. Bialik, O. M. *et al.* Availability and type of energy regulate the global distribution of neritic carbonates. *Scientific Reports 2023 13:1* **13**, 1–9 (2023).
75. Riera, R., Bourget, J., Allan, T., Håkansson, E. & Wilson, M. E. J. Early Miocene carbonate ramp development in a warm ocean, North West Shelf, Australia. *Sedimentology* **69**, 219–253 (2022).
76. Yoshii, K. *et al.* Origin of interstitial water beneath the continental shelf offshore northwestern Australia: insights from hydrogen and oxygen isotope compositions. *Prog. Earth Planet. Sci.* **12**, 1–23 (2025).
77. Hallock, P. Modern Coral Reefs Under Global Change: New Opportunities to Understand Carbonate Depositional Hiatuses. *The Paleontological Society Papers* **17**, 121–130 (2011).
78. Sosdian, S. M. *et al.* Constraining the evolution of Neogene ocean carbonate chemistry using the boron isotope pH proxy. *Earth Planet. Sci. Lett.* **498**, 362–376 (2018).
79. Gattuso, J. P., Frankignoulle, M., Bourge, I., Romaine, S. & Buddemeier, R. W. Effect of calcium carbonate saturation of seawater on coral calcification. *Glob. Planet. Change* **18**, 37–46 (1998).

80. Silverman, J., Lazar, B. & Erez, J. Effect of aragonite saturation, temperature, and nutrients on the community calcification rate of a coral reef. *J. Geophys. Res. Oceans* **112**, 5004 (2007).
81. Fabricius, K. E., Neill, C., Van Ooijen, E., Smith, J. N. & Tilbrook, B. Progressive seawater acidification on the Great Barrier Reef continental shelf. *Sci. Rep.* **10**, 1–15 (2020).
82. Mongin, M. *et al.* The exposure of the Great Barrier Reef to ocean acidification. *Nat. Commun.* **7**, 1–8 (2016).
83. Smith, J. N. *et al.* Shifts in coralline algae, macroalgae, and coral juveniles in the Great Barrier Reef associated with present-day ocean acidification. *Glob. Chang. Biol.* **26**, 2149–2160 (2020).
84. Lewis, E. & Wallace, D. *Program Developed for CO2 System Calculations*. https://www.osti.gov/biblio/1464255 (1998) doi:10.15485/1464255.
85. Nairn, M. G., Lear, C. H., Sosdian, S. M., Bailey, T. R. & Beavington-Penney, S. Tropical Sea Surface Temperatures Following the Middle Miocene Climate Transition From Laser-Ablation ICP-MS Analysis of Glassy Foraminifera. *Paleoceanogr. Paleoclimatol.* **36**, e2020PA004165 (2021).
86. Czarnota, K., Hoggard, M. J., White, N. & Winterbourne, J. Spatial and temporal patterns of Cenozoic dynamic topography around Australia. *Geochemistry, Geophysics, Geosystems* **14**, 634–658 (2013).
87. Christensen, B. A. *et al.* Indonesian Throughflow drove Australian climate from humid Pliocene to arid Pleistocene. *Geophys. Res. Lett.* **44**, 6914–6925 (2017).
88. Karatsolis, B. -Th., De Vleeschouwer, D., Groeneveld, J., Christensen, B. & Henderiks, J. The Late Miocene to Early Pliocene "Humid Interval" on the NW Australian Shelf: Disentangling Climate Forcing From Regional Basin Evolution. *Paleoceanogr. Paleoclimatol.* **35**, (2020).
89. Tagliaro, G. *et al.* Neogene siliciclastic deposition and climate variability on a carbonate margin: Australian Northwest Shelf. *Mar. Geol.* **403**, 285–300 (2018).
90. He, Y. & Wang, H. Terrestrial Material Input to the Northwest Shelf of Australia Through the Pliocene-Pleistocene Period and Its Implications on Continental Climates. *Geophys. Res. Lett.* **48**, e2021GL092745 (2021).
91. Samperiz, A. *et al.* Coastal seawater turbidity and thermal stress control growth of reef-building Porites spp. corals in Fiji. *Scientific Reports 2025 15:1* **15**, 1–15 (2025).
92. Gurnis, M., Kominz, M. & Gallagher, S. J. Reversible subsidence on the North West Shelf of Australia. *Earth Planet. Sci. Lett.* **534**, 116070 (2020).
93. Setter, R. O., Franklin, E. C. & Mora, C. Co-occurring anthropogenic stressors reduce the timeframe of environmental viability for the world's coral reefs. *PLoS Biol.* **20**, e3001821 (2022).
94. Vaes, B. *et al.* A global apparent polar wander path for the last 320 Ma calculated from site-level paleomagnetic data. *Earth. Sci. Rev.* **245**, 104547 (2023).
95. Van Hinsbergen, D. J. J. *et al.* A Paleolatitude Calculator for Paleoclimate Studies. *PLoS One* **10**, e0126946 (2015).
96. Schouten, S., Hopmans, E. C., Schefuss, E. & Sinninghe Damsté, J. S. Distributional variations in marine crenarchaeotal membrane lipids: a new tool for reconstructing ancient sea water temperatures? *Earth Planet. Sci. Lett.* **204**, 265–274 (2002).
97. Hopmans, E. C., Schouten, S. & Sinninghe Damsté, J. S. The effect of improved chromatography on GDGT-based palaeoproxies. *Org. Geochem.* **93**, 1–6 (2016).
98. De Vleeschouwer, D., Petrick, B. F. & Martínez-García, A. Stepwise Weakening of the Pliocene Leeuwin Current. *Geophys. Res. Lett.* **46**, 8310–8319 (2019).
99. Petrick, B., Reuning, L., Pfeiffer, M., Auderset, A. & Schwark, L. Sea surface temperatures governed the development and longevity of the Great Barrier Reef. Preprint at https://doi.org/10.21203/rs.3.rs-3054212/v1 (2023).
100. De Vleeschouwer, D. *et al.* Plio-Pleistocene Perth Basin water temperatures and Leeuwin Current dynamics (Indian Ocean) derived from oxygen and clumped-isotope paleothermometry. *Climate of the Past* **18**, 1231–1253 (2022).
101. Petrick, B. *et al.* High sea surface temperatures were a prerequisite for the development and expansion of the Great Barrier Reef. *Sci. Adv.* **10**, (2024).
102. Wuchter, C., Schouten, S., Coolen, M. J. L. & Damste, J. S. S. Temperature-dependent variation in the distribution of tetraether membrane lipids of marine Crenarchaeota: Implications for TEX86 paleothermometry. *Paleoceanography* **19**, (2004).
103. Zhang, Y. G. *et al.* Methane Index: A tetraether archaeal lipid biomarker indicator for detecting the instability of marine gas hydrates. *Earth Planet. Sci. Lett.* **307**, 525–534 (2011).
104. Kim, B. & Zhang, Y. G. Methane Index: Towards a quantitative archaeal lipid biomarker proxy for reconstructing marine sedimentary methane fluxes. *Geochim. Cosmochim. Acta* **354**, 74–87 (2023).
105. Sinninghe Damsté, J. S., Ossebaar, J., Schouten, S. & Verschuren, D. Distribution of tetraether lipids in the 25-ka sedimentary record of Lake Challa: extracting reliable TEX86 and MBT/CBT palaeotemperatures from an equatorial African lake. *Quat. Sci. Rev.* **50**, 43–54 (2012).
106. Sinninghe Damsté, J. S. Spatial heterogeneity of sources of branched tetraethers in shelf systems: The geochemistry of tetraethers in the Berau River delta (Kalimantan, Indonesia). *Geochim. Cosmochim. Acta* **186**, 13–31 (2016).
107. Auderset, A. *et al.* Enhanced ocean oxygenation during Cenozoic warm periods. *Nature* **609**, 77–82 (2022).
108. Zhang, Y. G., Pagani, M. & Wang, Z. Ring Index: A new strategy to evaluate the integrity of TEX 86 paleothermometry. *Paleoceanography* **31**, 220–232 (2016).
109. Hernández-Sánchez, M. T., Woodward, E. M. S., Taylor, K. W. R., Henderson, G. M. & Pancost, R. D. Variations in GDGT distributions through the water column in the South East Atlantic Ocean. *Geochim. Cosmochim. Acta* **132**, 337–348 (2014).
110. Taylor, K. W. R., Huber, M., Hollis, C. J., Hernandez-Sanchez, M. T. & Pancost, R. D. Re-evaluating modern and Palaeogene GDGT distributions: Implications for SST reconstructions. *Glob. Planet. Change* **108**, 158–174 (2013).

Figures

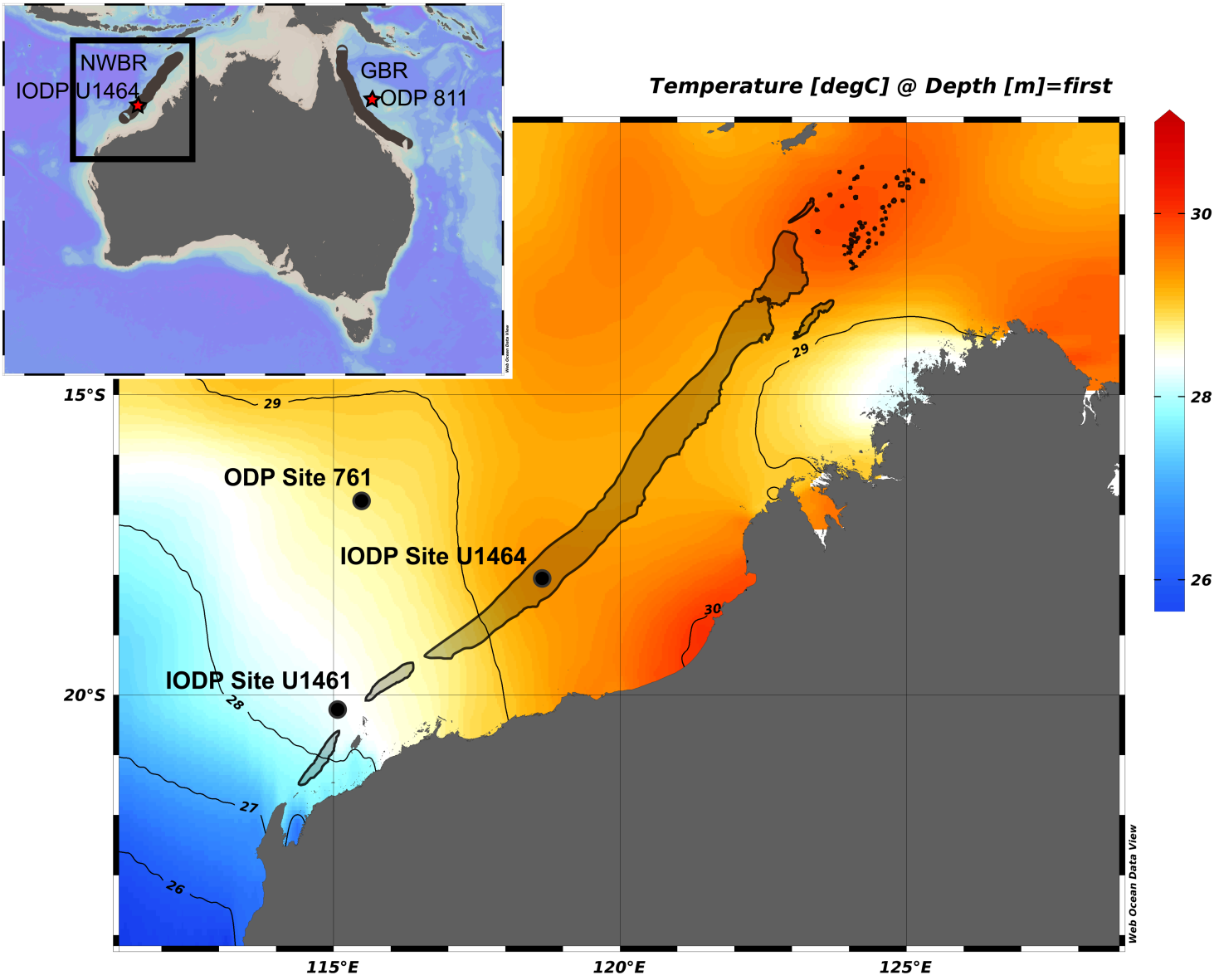


Figure 1

Map showing summer SST (January-March) based on the World Ocean Atlas 2023, based on data for the last 50 years [25]. The map was created using Ocean Data View [26]. The location of the Miocene barrier reef (grey) is based on [20]. The sites for which data is shown in this study are indicated by black dots. The insert map shows the site of the Northwest Shelf Barrier Reef (NWBR) and the Great Barrier Reef (GBR) (both black lines), and the location of ODP Site 811 (red star).

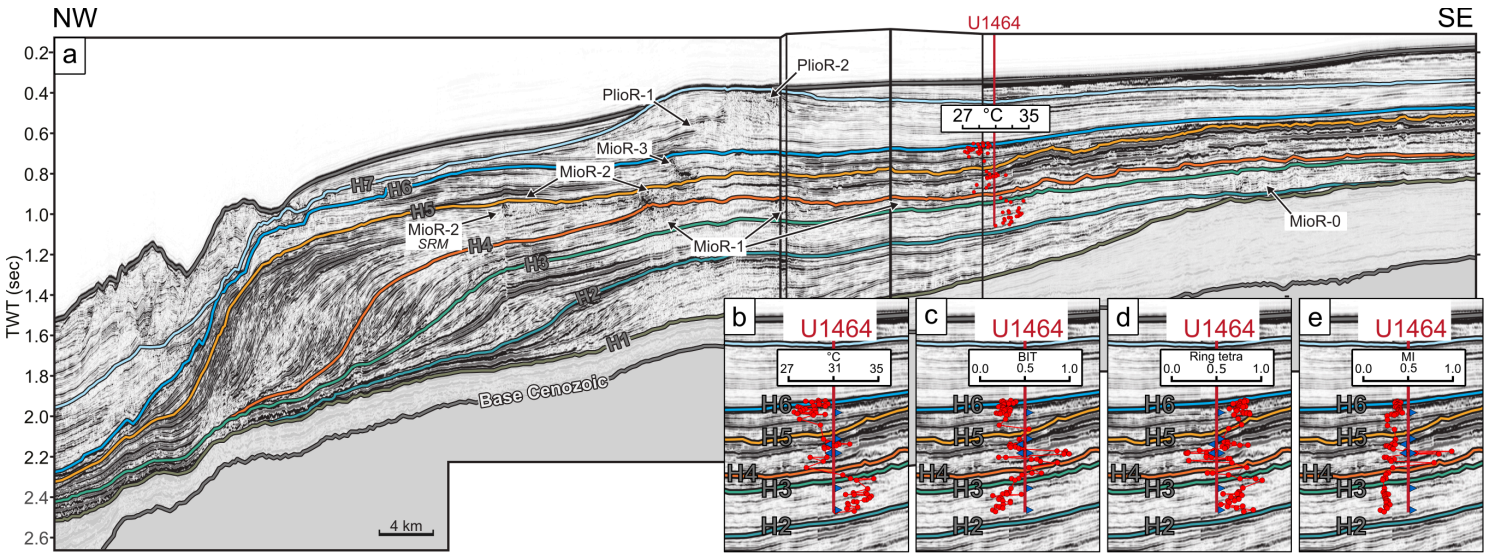


Figure 2

a) Seismic section from [19,20], with b) the TEX_{86}^{H} -derived SSTs and major GDGT indices c) BIT, d), #ring tetra, and e) MI plotted downcore. The location of the Miocene reefs is shown (MioR-0 to MioR3). H numbers represent interpreted seismic horizons, which can be linked to major steps in reef development (see Fig. 3). Blue triangles mark the positions of photographs shown in Figures S3 and S4.

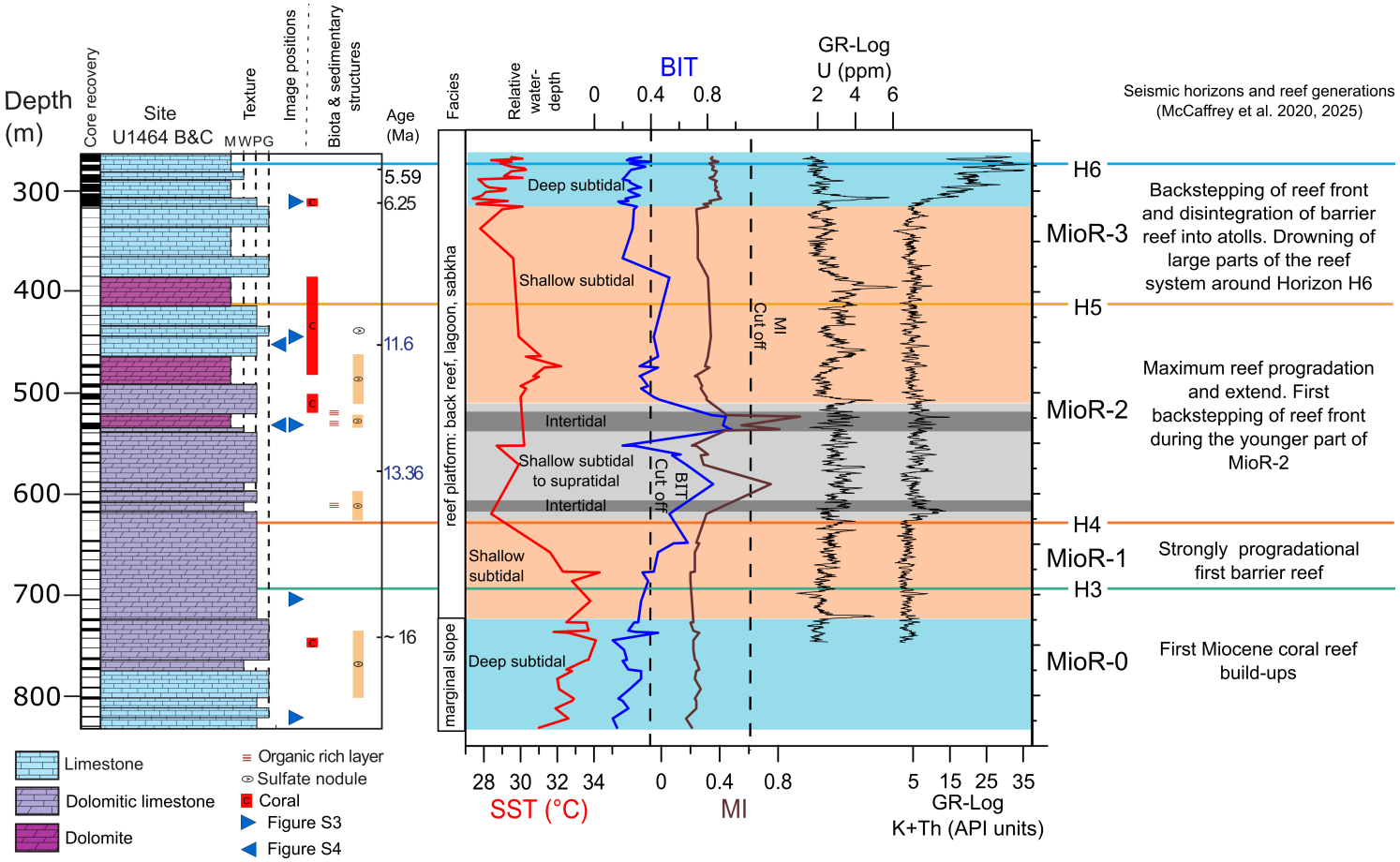


Figure 3

Lithologic column based on shipboard descriptions of the core, presence of traces of corals in the core, and sedimentary structures. Triangles indicate the positions of core photos and thin sections shown in the supplements (Figs. S4, S5). The age model is based on [27,34]. This is compared to the biomarker record (TEX_{86}^{H}, BIT, and MI indices). The reef generations (MioR) and seismic horizons H3 to H6 are from [20]. The spectral GR log data are from the shipboard logging [35], and the facies interpretation in this study is based on seismic interpretation and core analysis.

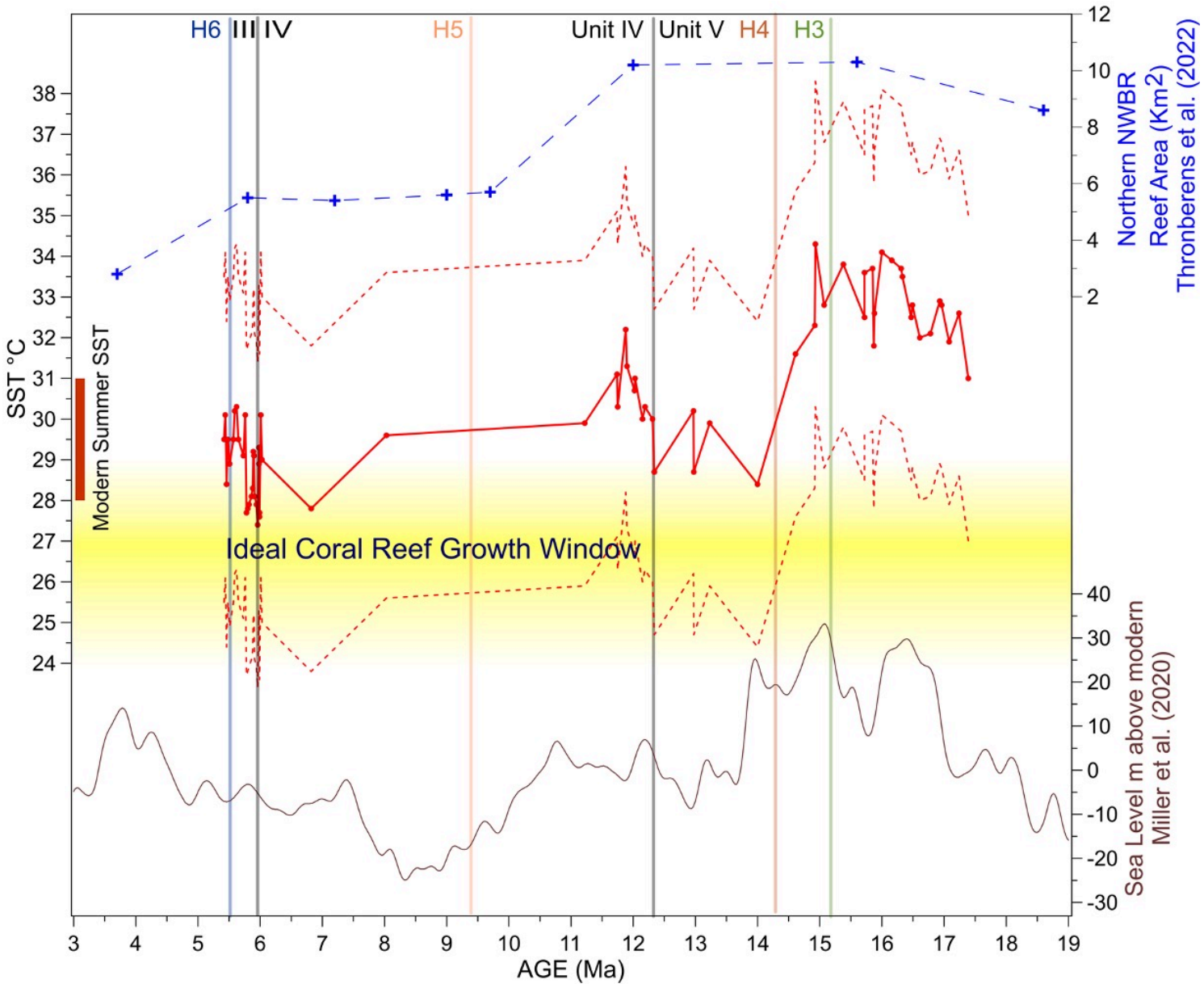


Figure 4

Areal extent of the NWBR in the Browse Basin based on 3D seismic data (blue dotted lines) [24]. Unit boundaries (black lines) are from [35] and the seismic horizons (colored lines) are from [19,20] (See figures 2, 3). Temperature reconstruction (in red), with the 2.5 °C uncertainty in GDGT-SST reconstruction [43] indicated by red dashed lines above and below. The yellow box represents the published modern ideal coral reef growth window of 25 to 29°C [44,45]. Global eustatic sea-level changes are shown at the bottom [46].

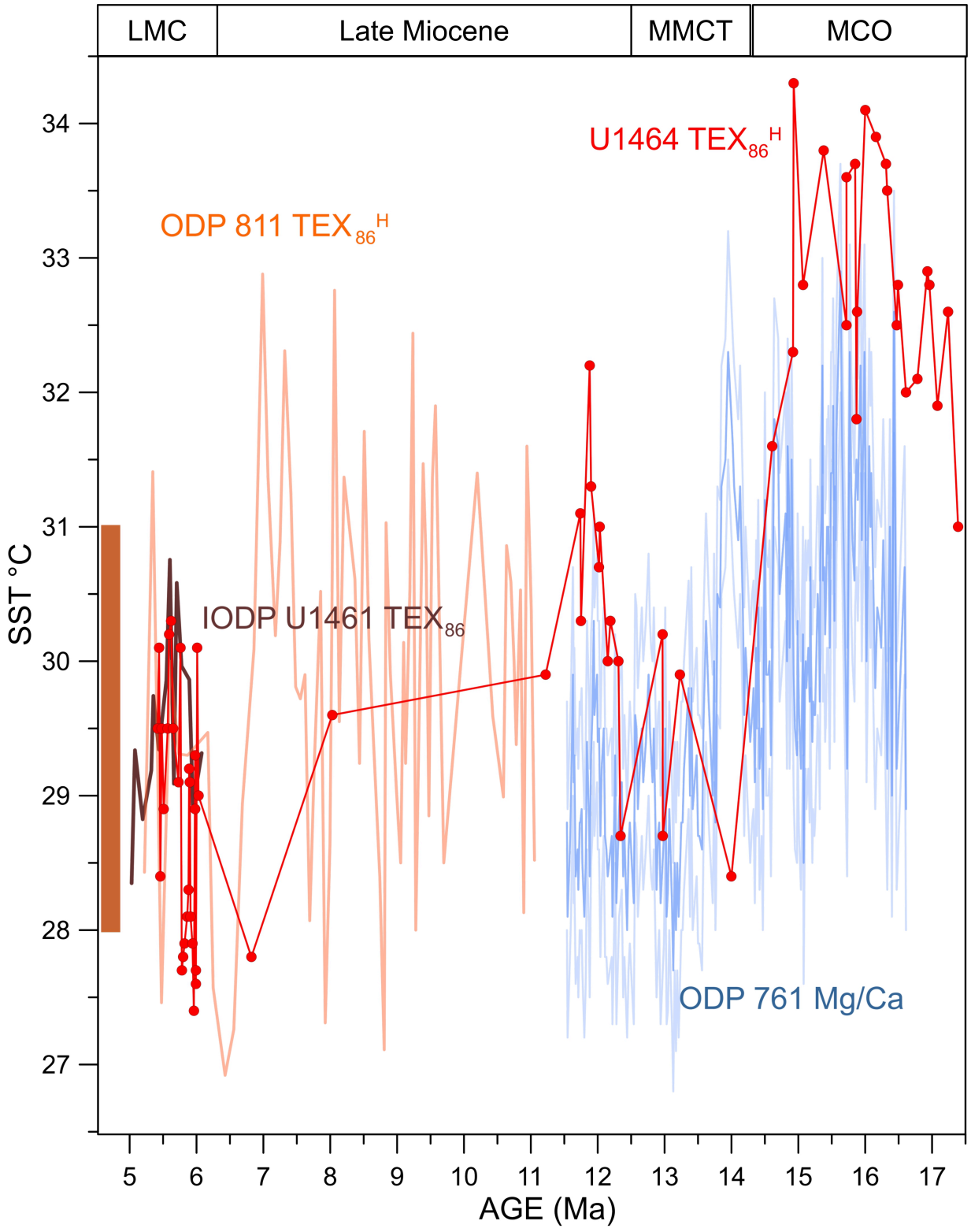


Figure 5

TEX_{86}^{H} derived SST data from IODP site U1464 (red) compared to the Mg/Ca-derived SST record from nearby ODP Site 761 (the dark blue line represents the best reconstruction of Mg/Ca-derived SST, whereas light blue lines represent varying salinity scenarios (constant modern, constant modern +1 PSU, and constant modern −1 PSU) [47]. The ODP Site 811 TEX_{86}^{H}-derived SST is shown in light orange [16,48]. The IODP site 1461 TEX86H data is shown in brown [49]. The brown bar on the side represents modern summer SSTs [25]. The significant climatic periods are shown above.

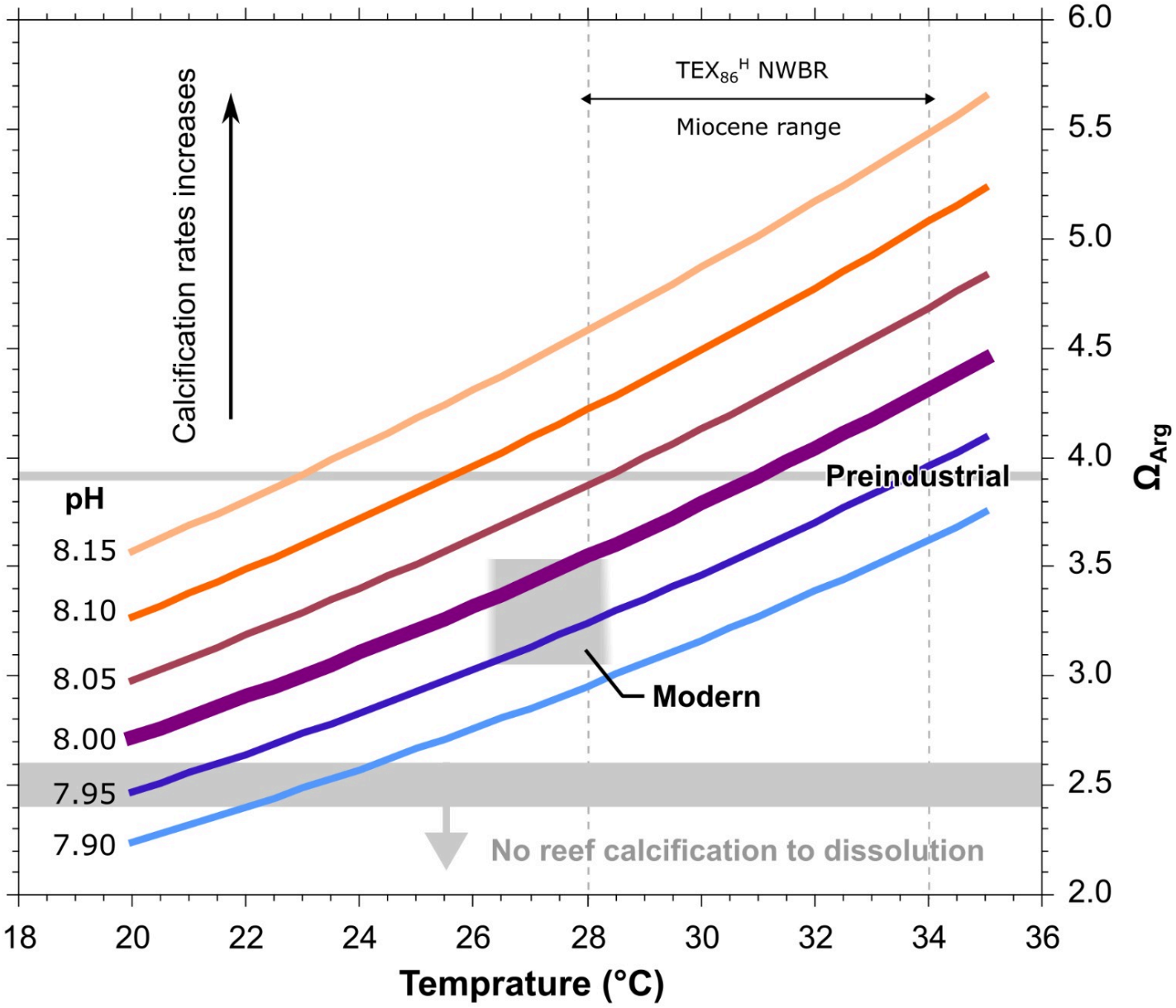


Figure 6

Change in aragonite saturation (Ω_{arg}) as a function of temperature for different pH values assuming conservative alkalinity of ~2400 µmol kg^{-1}. The modern pH of the Great Barrier Reef is based on [81], [82], and [83]. A surface pH of ~8 is likely for the study period [78]. The range of calcification succession follows [80]. Values were calculated using CO2SYS [84].

Supplementary Files

This is a list of supplementary files associated with this preprint. Click to download.

- NCSupplement.docx